DOI: 10.1002/marc.((insert number)) ((or ppap., mabi., macp., mame., mren., mats.))

Full Paper

Scaffolds of hyaluronic acid-poly(ethyl acrylate) interpenetrating networks: characterization and in vitro studies

E. Rodríguez-Pérez[1], A. Lloret Compañ[1], M. Monleón Pradas[1,2,*], C. Martínez-Ramos[1]

_____

M.Sc. E. Rodríguez-Pérez[1,#], Ph.D. C. Martínez-Ramos[1,#], M.Sc. A. Lloret Compañ[1], Prof. M. Monleón Pradas[1,2]
[1] Center for Biomaterials and Tissue Engineering, Universitat Politècnica de València, 46022, Valencia, Spain
[2] Networking Research Center on Bioengineering, Biomaterials and Nanomedicine, (CIBERBBN), Valencia, Spain
E-mail: mmonleon@ter.upv.es

_____

Hyaluronic acid (HA) provides many advantages to regenerative implants through its bioactive properties, but it also has many limitations as a biomaterial if it's not chemically modified. In order to overcome some of these limitations, HA has been combined with poly(ethyl acrylate) (PEA) in the form of interpenetrating polymeric networks (IPNs), in which the HA network is crosslinked with divinyl sulfone (DVS). Scaffolds of this IPN have been produced through a template-leaching methodology, and their properties have been compared with those of single-network scaffolds made of either PEA or crosslinked HA. A fibroblast cell line has been used to assess the in vitro performance of the scaffolds, revealing good cell response and a differentiated behaviour on the IPN surface when compared to the individual polymers. Altogether, the results confirm that this type of material offers an interesting microenvironment for cells, which can be further improved towards its potential use in medical implants.

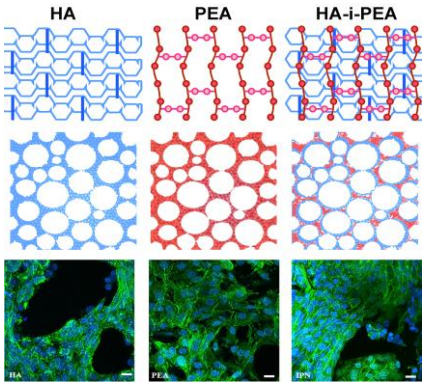
HA
PEA
HA-i-PEA

1. Introduction

Tissue engineering combines cells and biochemical and/or physical signals with scaffolds targeting regeneration of tissues.[1] In some cases, the biomaterial used as a scaffold can be designed to perform multiple functions, including biochemical signalling in biological processes, either regenerative, immunological or others.[2] The use of hyaluronic acid (HA) as a material in regenerative implants is of interest because it is a major component of the extracellular matrix in many tissues and has many outstanding biological properties. Among other effects, HA has been shown to regulate immune and inflammatory response,[3-5] cell differentiation,[6] vascularisation,[7-8] scar tissue formation,[4, 9] cell adhesion to matrix proteins,[10] and interacts with many signalling pathways through specific cell receptors.[11]

However, biomaterials made exclusively from HA present several features that may be detrimental to some extent; features such as limited cell adhesion [10, 12-13] and poor mechanical properties.[14-15] The former can be addressed by functionalizing the HA molecule in order to incorporate adhesion motifs,[16] or combining it with other molecules which do have cell adhesion capacity.[17] Both mechanical properties and manipulability of HA can be improved by covalent crosslinking[18-20] or by using it as a filler or coating material in composite scaffolds.[12] Functionalization and covalent modification of the molecule alter some of the HA's molecular properties,[21-24] whereas physical combination with other materials allows to preserve these properties.[7, 17, 25] Here we present a hitherto unexplored way of physical combination of HA with a second polymer: the formation of interpenetrating networks, IPNs, in the form of macroporous scaffolds. IPNs are polymeric materials made from two chemically independent networks, which interpenetrate at a molecular or microscopic scale.[26] These systems represent a way to synergistically combine properties of different materials without altering their individual chemical identity. Here we take advantage of the micro- and nanoporosity created in HA by lyophilization to fill up those pores with the precursor of the second network, which is polymerized afterwards. Our methodology,

moreover, allows producing scaffolds by the template-leaching technique. We have thus obtained IPN of crosslinked HA and crosslinked PEA, HA-i-PEA, conformed as scaffolds. Poly(ethyl acrylate) has properties opposite, or complementary, to those of HA: it is a biostable elastomer, with very low hydrophilicity, and very good cell-adhesion properties. It has revealed good biological performance both *in vitro*[27-29] and *in vivo*.[30-31] The combination of HA and PEA should thus deliver a system with intermediate swelling capacity, cell-adhesion, mechanical properties and degradation rates. In the present study, HA-i-PEA scaffolds were produced and characterized. Biocompatibility of the materials was assessed *in vitro* by carrying out cytotoxicity and viability studies with an L929 fibroblast cell line, while cell morphology on the surface of the scaffolds was studied via immunochemistry and microscopy imaging.

2. Experimental Section

2.1. Preparation of scaffolds

2.2.1. Preparation of hyaluronic acid porous scaffolds

Hyaluronic acid sodium salt from *Streptococcus equi* (1.5-1.8 MDa; Sigma-Aldrich) was dissolved overnight to a 5% (w/v) in 0.2 M NaOH (aq). Then, divinyl sulfone (DVS, Sigma-Aldrich) was added to this solution up to a concentration of 1.4% (w/v). Once homogenized, the solution was vaccuum-injected into moulds made from sintered beads of poly(ethyl methacrylate) (PEMA, Elvacite® 2043, Lucite International, Inc.). These beads had an approximate diameter of 200 μm. The crosslinking reaction of HA with DVS was left to complete for an hour and a half, and then the filled moulds were stored at -20 °C for two hours before lyophilization. PEMA templates were removed by leaching using boiling ethanol in a Soxhlet reflux for 24 h. Afterwards, HA scaffolds were immersed in distilled water for 3 h, frozen at -20 °C for another 2 h and then lyophilized. All scaffolds were cut into discs with 5 mm diameter.

2.2.2. Preparation of poly(ethyl acrylate) scaffolds

A homogenized mixture containing 97% (wt%) ethyl acrylate (EA, Sigma-Aldrich), 2% ethylene glycol dimethacrylate (EGDMA, Sigma-Aldrich) and 1% benzoin (Scharlab, Barcelona, Spain) was injected into porous templates made from sintered poly(methyl methacrylate) beads (PMMA, Colacryl DP300U®, Lucite International, Inc.) These beads had an approximate diameter of 120 μm. After injection, the moulds were exposed to UV light overnight in a sealed chamber in order to produce the polymerization reaction. Afterwards, they were put in an oven at 90 °C for 12 h in order to complete the reaction and minimize unreacted residues. Templates were removed from the resulting materials via the solvent-leaching technique in a Soxhlet reflux apparatus, using acetone in 4 cycles of 8 hours. Finally, scaffolds underwent gradual solvent exchange from acetone to water before drying them under vacuum, in order to prevent pore collapse. Scaffold discs with a diameter of 5 mm were cut from the obtained materials.

2.2.3. Preparation of interpenetrating polymer networks scaffolds of hyaluronic acid and poly(ethyl acrylate), HA-i-PEA

Hyaluronic acid sodium dissolved in NaOH (aq) together with DVS, as described in 2.1.1., was vaccuum-injected into moulds made from sintered beads of poly(ethyl methacrylate), as described previously. After the cross-linking reaction had taken place, and without removing the PEMA template, the materials were soaked in a homogenized mixture of 1% (wt%) benzoin, 2% EGDMA and EA monomer diluted to a 60% (wt%) in ethanol. The materials were left in a UV chamber overnight in order to produce the polymerization of PEA in the micropores of the HA network. The HA-i-PEA networks thus produced were put in a Soxhlet reflux apparatus for 24 hours using ethanol as solvent in order to remove the porogenic template. Then, the ethanol-soaked IPN scaffolds were gradually hydrated and then kept for 2

hours in distilled water, before being frozen at -20 °C for another 2 hours and lyophilized. All scaffolds were cut into discs with 5 mm diameter.

2.2. Characterization of scaffolds

2.2.1. Scanning electron microscopy

Samples were dried, glued onto sample holders and sputter-coated with gold in a vacuum chamber. SEM images were obtained at 15 kV of acceleration voltage and 15 mm of working distance in a JSM-5410 microscope (Jeol, Tokyo, Japan). Images obtained at 100X magnifications were processed with the ImageJ / FIJI software [32] in order to obtain the average pore diameter from each type of scaffold, by applying the *Nearest neighbor Distance* Plug-In (NnD, by Yuxiong Mao). Additionally, swollen IPN scaffold samples were observed through cryoSEM in a JSM5410 (JEOL Ltd, Tokyo, Japan) instrument equipped with a CT 1500 cryo-unit (Oxford Instruments, Abingdon, United Kingdom).

2.2.2. Density measurements

Density values (ρ) from dry scaffold sample discs were determined gravimetrically, applying Archimedes' principle. First, each scaffold sample was weighed in Mettler AE 240 balance (Mettler-Toledo Inc., Columbus, OH, USA) air (m_{air}) and then immersed in n-octane (m_{oct}), having been previously vacuum-filled with n-octane, if necessary (the case of PEA). Then, density values were obtained with the equation:

$$\rho_{sample} = \frac{m_{air}}{m_{air} - m_{oct}} \rho_{oct} \quad (1)$$

2.2.3. Porosity determination

Porosity values from dry samples of all types of scaffolds were determined gravimetrically by weighing each sample in air, before (m_{air}) and after filling their pores with n-octane (m'_{air}),

assuming that there is no swelling by octane neither for HA nor for PEA polymeric networks. Afterwards, octane-filled scaffolds were weighed in octane (m_{oct}), and porosity values were obtained with the following equation:

$$\varphi = \frac{V_{pore}}{V_{scaff}} = \frac{V_{pore}}{V_{bulk}+V_{pore}} = \frac{m'_{air}-m_{air}}{(m_{air}-m_{oct})+(m'_{air}-m_{air})} \quad (2)$$

2.2.4. Thermogravimetric analysis (TGA)

Samples with a mass of approximately 5 mg were processed in a SDT-Q600 apparatus (TA-instruments, USA), monitoring mass loss while heating up to 900 °C at a rate of 10 °C min^{-1} under a N_2 flow with a constant flow-rate of 50 mg min^{-1}. In order to remove strongly-bonded water molecules from HA chains, a previous step was carried in a N_2 atmosphere by heating the sample up to 100 °C at 10 °C min^{-1} and maintaining this temperature for 10 minutes before leaving the sample to cool down back to 30 °C. Three replicas were measured for each type of scaffold.

2.2.5. Elemental analysis

Elemental compositions of scaffolds (n = 3 for each type of sample) were obtained through EDS (energy dispersive X-ray spectroscopy). Data were acquired in a FESEM apparatus (Carl Zeiss Ultra 55, Germany). Primary electron voltage was set to 10 kV. 5 measurements were made on different areas of each sample in order to obtain their average elemental composition.

2.2.6. Swelling tests

Scaffold sample discs of each material were weighed before and after soaking them in PBS 1X at 37 °C for increasing time periods, until they reached weight equilibrium. Water content (WC) was expressed as:

$$WC = \frac{(m - m_0)}{m_0} \quad (3)$$

2.2.7. Mechanical tests

Scaffold samples were cut to bars of approximate dimensions 2 × 1 × 1 mm. Stress-strain tests under constant stretching rate of 5 mm·min^{-1} were conducted in a TMA / S6000 machine (Seiko Instruments Inc.). Measured values of deformation ΔL and force f were converted to strain $\varepsilon = \Delta L/L_0$ and stress $\sigma = f/A$ values using the initial length L_0 and cross-sectional area A values of the samples.The tensile Young modulus (E) was determined from the initial slope (up to 0.05 strain) of the stress-strain curves.

2.3. Degradation assays

Samples were dried and weighed before and after immersion for increasing time periods in three different media: an acidic solution made from HCl (BioReagent, from Sigma Aldrich) in PBS 1X (prepared from powder, Sigma Aldrich), stabilized at pH 4; a hyaluronidase solution with 10 U ml^{-1} of the enzyme (obtained from bovine testes, Sigma Aldrich), 300 mM citric acid (Sigma Aldrich), 150 mM Na_2HPO_4 (Scharlab), 150 mM NaCl (Panreac, Barcelona, Spain) stabilized at pH 6.3; and a PBS 1X solution (prepared from powder and stabilized at pH 7.4, Sigma Aldrich). The degree of degradation was measured as the fraction of initial mass lost throughout the degradation experiment. A fast degradation study was carried out using a concentrated solution of HCl (ACS reagent, pH0.1) for 48 hours. Degradation media were kept at 37 °C during all the experiments. Samples degraded in concentrated HCl were observed by cryoSEM in a JSM5410 (JEOL Ltd) instrument equipped with a CT 1500 cryo-unit (Oxford Instruments). Samples were fixed vertically in a metallic sample holder and cryofractured using liquid nitrogen in order to reveal their internal structure. All samples were

maintained in high vacuum, allowing for complete water sublimation before observing them at 15 kV and 15 mm of working distance.

2.4. *In vitro* studies

2.4.1. Cytotoxicity assay

An indirect cytotoxicity assay was made using L929 mouse fibroblasts obtained from subcutaneous adipose, connective and areolar tissues (Sigma-Aldrich) taken to the 9th passage. The used medium was Dulbecco's Modified Eagle Medium (DMEM) with high glucose content (4,5 g L^{-1}), from Invitrogen (Thermo Fisher Scientific, Waltham (MA), United States), supplemented with 10% Fetal Bovine Serum (FBS, Thermo Fisher Scientific). Samples were sanitized with ethanol and sterile water before use. In order to obtain the extract from each sample type (PEA, HA and IPN), 1ml of medium per gram of sample was used to incubate each replicate sample for 24h in a humidified incubator at 37 °C and 5% CO_2.

Meanwhile, 96-well plates were seeded with 1 x 10^4 cells/well and incubated with fresh medium for 24 h at 37 °C and 5% CO_2; then that medium was replaced with extracts from samples, using fresh medium as a negative control and latex extract as a positive control. After 24, 48 and 72 hours, all cultures were tested with an MTT assay. First, extracts and control mediums were removed, then all samples were washed with PBS 1X and cells were incubated with 100µl per well of MTT medium prepared with 90% DMEM (vol%) and 10% of a stock solution containing 1 mg ml^{-1} MTT. Plates were returned to incubation in darkness for 2.5 h. Afterwards, the MTT medium was replaced with 120µl per well of isopropanol before shaking the plates for 1 min, then 100µl of this isopropanol was removed from each well and transferred to another 96-well plate in order to read Formazan absorbance at 550 nm in a Victor Multilabel Counter 1420 (Perkin Elmer, Waltham (MA), United States). Three replicates were made from each sample, blank and negative and positive controls.

2.4.2. Cell proliferation and scaffold colonization

Cell colonization and proliferation of the different materials were assessed through *in vitro* cultures using L929 fibroblast cells. Three replicas for each material plus three polystyrene covers as positive controls were placed in 48-well plates. Prior to cell culture, samples were washed with a PBS solution at pH 7.4 and then were left to acclimate in medium overnight. Then, 2 x 10^4 cells suspended in 20 µl of medium were seeded on the upper-side of each material and incubated for 30m at 37 °C and 5% of CO_2 in order to allow for initial cell adhesion. Afterwards, 400 µl of DMEM supplemented with 10% FBS and 1% of a penicillin/streptomycin antibiotic mix was added. Medium was renewed every 2 days until cultures were halted.

The MTS assay was made with cultures at day 1, 5 and 10; using three replicas for each measurement. First, a MTS solution was prepared by adding 1 µl of MTS reactive for each 5 µl of phenol-red-free DMEM medium. Then, culture medium was removed from all samples and they were washed once with a PBS 1X solution before adding 400 µl of MTS solution on each well. After 2 h incubation, the reacted MTS solution was removed from each well and divided into 3 different wells before reading their absorbance values at 490 nm in a Victor Multilabel Counter 1420 (Perkin Elmer, Waltham, MA, USA).

2.4.3. Immunofluorescence microscopy

L929 cultures at day 10 were treated with 4% paraformaldehyde (Panreac) for 20 min, washed with a phosphate buffer (PB) solution and then kept 1h at room temperature in 10% FBS and 1% Triton X-100 (Aldrich) in PB. Afterwards, they were incubated for 1h in a 1:200 dilution of Phallacidin Bodipy FL (Invitrogen) with 1% bovine serum albumin (BSA; Aldrich, 35% purity) in PB at room temperature and in the dark. Finally, samples were stained with 1:5000 4,6-diamidino-2-phenylindole dihydrochloride (DAPI; Sigma-Aldrich) solution for 10 min, followed by two PB rinses. After this staining protocol, samples were mounted in glass

microscope slides applying Fluorsave reagent (Merck Milipore, Billerica (MA), United States), coverslipped and examined with a Nikon eclipse 80i fluorescence microscope, and a confocal laser scanning microscope (CLSM, Zeiss 780 Axio observer z1, Carl Zeiss AG, Oberkochen, Germany).

2.4.4. Processing of cell culture samples for SEM imaging

Cells cultured in scaffolds were fixed with a 3% glutaraldehyde solution containing phosphate buffer saline (PBS 1X) for 60 min at 37 ºC and post-fixed with 1% osmium tetroxide (OsO_4, Aname) for 2 h at room temperature followed by four rinses with distilled water. Samples were then dehydrated in increasing ethanol concentrations and prepared for SEM imaging as mentioned in section 2.4.

2.5. Statistical analysis

Results are expressed as average ± standard deviation from at least three replicates. Data was analyzed pair wise with the ANOVA test using the Statgraphics Centurion XVI.I software. Significance was assigned at p-values < 0.05. Statistically significant differences are shown in the results.

3. Results and Discussion

3.1. Characterization of scaffolds: morphology, density, porosity, swelling and tensile

SEM images from the three types of scaffolds produced (Figure 1) show an internal porous structure with good interconnectivity and regularity in all samples. PEA scaffolds possess a mean pore diameter of 104±18µm, while the HA and IPN ones have pores in the range of 174±32µm and 182±20µm, respectively, as determined by image processing. These differences are due to the different size of the beads used as porogenic templates in each case.

Also, while some pore shrinking in the HA and the IPN scaffolds might take place after removal of water, that effect could be slightly offset in the IPN by the structural

reinforcement provided by PEA. Pore volume fraction and density values of the scaffolds are given in Table 1. The density of the IPN is comprised between those of the single-network materials (HA and PEA). This is also true for the EWC values after immersion in water (Table 1). While the WC in PEA mostly corresponds to water retained in the scaffold's pores and does not increase with time, WC values from HA and IPN scaffolds do rapidly increase in the first hour after immersion and then increase more slowly until reaching equilibrium at days 3-5. WC values are always lower in IPN scaffolds, when compared to HA ones (Figure 2B).

Stress-strain curves (Figure 3) show the different mechanical behaviour of the three types of scaffolds. The Young moduli (*E*) obtained from these curves of all three types of scaffold (Table 1) confirm that the incorporation of PEA (0.83±0.09 MPa) represents a mechanically reinforcement of the IPNs (0.28±0.04 MPa) when compared to the HA scaffolds (0.05±0.02 MPa).

Cryo-SEM images taken from swollen IPN samples show two differentiated networks intermingled within the porous structure of the scaffold, the HA network forming a mesh between multiple PEA laminae (Figure 4C and 4D). These cryo-SEM micrographs by themselves cannot help decide whether the PEA network does or does not form a continuous structure through the scaffold, although SEM images (Figure 1) reveal an increase in the diameter of the trabeculae in HA-i-PEA scaffolds when compared to HA scaffolds. On another hand, swollen HA-i-PEA scaffolds show a smaller linear swelling ratio than HA ones (see thickness values in Table 1).

HA-i-PEA networks are biphasic materials with reduced EWC compared with HA, which is to be expected due to the hydrophobic nature of the PEA network that contributes to the dry mass of the scaffolds. Polymerization of the PEA network was carried in a UV chamber, and that may have caused a partial degradation of the high molecular weight chains of HA.[33] This, added to a second lyophilization process –which has also been associated to

cleavages in HA chains–,[34-36] may be responsible for an additional loss of swelling capacity of the HA network in HA-i-PEA scaffolds.[33, 37] Besides, the presence of a PEA network might cause a reduction in the absorption of water by the IPN scaffolds by producing a physical and/or mechanical constraint in the volumetric swelling of the HA network. After a partial degradation of the HA network of the IPN, cryo-SEM images of swollen samples (Figure 4C and 4D) reveal that PEA forms multiple laminae intermingled with the HA network. To note is that cryo-SEM images after advanced degradation of HA (Figure 4E and 4F) show not only PEA laminae but also many filamentous residues of PEA, which could have polymerized within hollow channels created inside HA trabeculae after the first lyophilization step.

3.2. Characterization of scaffolds: composition as deduced from TGA, densities and quantitative EDS

Thermal degradation of the samples was measured by TGA, and the residual mass was plotted against temperature (Figure 2A). Both HA and PEA present a main thermal decomposition step, near 240°C and 400°C. In the case of IPN samples, both steps appear without any temperature shift, and no other degradation processes can be detected. Residual masses from samples (m) at different temperatures were used in order to estimate the mass fraction of PEA (ω_{PEA}) in IPN samples, by comparing this residue with those of HA and PEA samples, assuming no interference between their respective degradation processes (as seen in the TGA derivative graph, Figure 2A), and using the following equation:

$$m_{IPN} = m_{PEA} \cdot \omega_{PEA} + m_{HA} \cdot (1 - \omega_{PEA}) \quad (4)$$

where the residual mass values are always taken at the same temperature. The calculated composition values varied depending on which temperatures were used for obtaining the

residual mass values. For example, ω_{PEA} calculated from residual masses at 800°C (where practically all PEA has disappeared) results in a value of 23.43±4.50%, in line with the 23.07±0.85% obtained from 240°C masses, while residual masses at 500°C give a ω_{PEA} value of 12.23±0.83%. These conflicting composition values might be related to differences in the diffusion of volatile residues from the PEA network between IPN and PEA samples. The composition value obtained from residual masses at 800°C, when the PEA network is completely degraded, was chosen as the most reliable. At 800°C the HA has a quantifiable residue and the PEA network is completely degraded. However, this determination is not free from uncertainty, since small HA fragments may be blown by the gas flow during the analysis.

In order to have an independent estimate of composition, EDS analysis was performed on the different samples (Table 2). Assuming no contamination of the samples, the presence of elemental nitrogen (N) in IPN scaffolds is directly related to its HA contents, which may then be quantified by comparing the N signals of PEA, HA and IPN samples, by using the equation:

$$\boldsymbol{N_{IPN} = N_{PEA} \cdot \omega_{PEA} + N_{HA} \cdot (1 - \omega_{PEA})} \quad (5)$$

with $\boldsymbol{N}$ being the average mass fraction of elemental N as quantified through EDS. According to this, the presence of elemental N in IPN samples is consistent with the composition calculated through the TGA experiments, giving a 24.0±0.7% of PEA in mass.

The two-step method described here permitted to obtain highly porous scaffolds with a template-leaching technique. The micropores generated by lyophilization of water crystals in the HA hydrogel are efficiently occupied by the EA monomer, which upon polymerization yields a PEA hydrophobic network entrapped within the hydrophilic HA network of the IPN. Thus a sequential IPN results.[26, 38] The connectivity of this PEA is dependent on the

morphology of the water crystal network generated before lyophilization, especially on its connectivity. The topological features of the PEA network in the IPN may depend on factors such as the initial amount of water in the HA network, the formation of water crystals (creating pores and channels within the HA) in the freezing processes prior lyophilization, the crosslinking density of the HA polymer (which also influences water crystalization) and on the concentration of the reactive EA mixture injected in the lyophilized interstices. Producing IPN with higher ω_{PEA} values may be possible by decreasing the crosslinking density of HA, increasing its equilibrium water content prior lyophilization, and/or increasing the concentration of the EA monomer (by reducing its dilution).

3.3. Degradation studies

In a time lapse of 4 weeks, no degradation is appreciated in PEA samples, neither in PBS (Figure 4B) nor in hyaluronidase medium (Figure 4A), while HA samples lose mass in a range comprised between 5-10% in PBS, and 10-15% in hyaluronidase. IPN samples show a smaller degree of degradation than HA (Figure 4A); the observed differences between them being consistent with the estimated PEA mass fraction in the IPN (0.23±0.04), except for day 28 of degradation in hyaluronidase medium, where HA degradation becomes more accentuated in comparison.

A fast degradation experiment was carried out by immersing the samples in a strong acidic HCl solution (pH≈0.1) during 48h in order to obtain the PEA residue in the IPN samples after the complete removal of HA, using HA scaffolds as positive degradation controls. PEA scaffolds presented no appreciable loss of mass after 48h. The IPN residue was not manageable for weighing or preparation for SEM imaging, suggesting that the PEA network was not continuous throughout the scaffolds for this PEA mass fraction in the IPN. Hence, the degradation was carried only for 24h, at a point where most of the HA network was degraded but still present to allow manipulation of the sample as a whole. Samples were

then observed through cryoSEM and compared with non-degraded IPN samples previously swollen in water (Figure 4E and 4F), revealing that IPN residues after degradation consist of microscopic independent filaments and laminae (all presumably from the PEA network), held together by the remaining HA. The cryoSEM images of the swollen, non-degraded IPN do not show the filaments (Figure 4C and 4D).

These degradation experiments reveal that the HA scaffolds (and also the IPN ones) are particularly resistant to degradation by hyaluronidase, at least under the described protocols. The high HA/DVS molar ratio used in the synthesis of HA scaffolds (close to 1:1) gives rise to a high crosslinking density of the HA network which leads to a reduced enzymatic degradability, as seen in other studies.[15] On another hand, the exposure of HA-i-PEA to UV light during PEA polymerization may result in the creation of HA oligomers in the hydrogel that should increase its degradability.[20] The lyophilization stages involved in the fabrication of the scaffolds (one stage for the HA scaffolds, two for the HA-i-PEA ones) may also have an effect on the degradability of HA, in the sense of reducing its kinetics.[36]

3.4. *In vitro* studies: viability, proliferation and cell colonization of scaffolds

In indirect cytotoxicity assays, IPN extracts had smaller values of viability at 24 h and 48 h than those of the positive control (fresh medium, set as a 100% cell survivability value), but at 96 h all types of samples reached and even surpassed the levels of cell viability obtained from the positive control (Figure 5). Optical microscope images show no appreciable differences between L929 fibroblasts cultured with 96 h extracts, except for the negative control where cells appear in lower densities.

The template-leaching method here described was effective for producing scaffolds of HA-i-PEA IPN with a highly regular and interconnected pore structure, making them easily colonisable by the seeded cells. In order to quantify the proliferation of adherent L929 cells on PEA, HA and IPN scaffolds, an MTS cell viability assay was performed. After 1 day of

incubation, no difference in cell proliferation could be appreciated between the different substrates (Figure 6). At days 5 and 10, cell metabolic activity in the HA and IPN scaffolds was significantly higher than in PEA, with IPN scaffolds showing the highest index of metabolic activity. This may be unexpected, since PEA is more cell-adherent than HA .[39] A number of reasons may be responsible for this finding. First, the lower porosity of PEA samples (62% pore volume fraction, against 96-97% for the HA and HA-i-IPN scaffolds), together with their comparatively smaller total volumes after swelling may account for a reduction of the available surface for cells in the case of PEA scaffolds: according to the thickness data of Table 1, the linear swelling ratio of the samples was Λ_{PEA}=1.00, Λ_{HA}=1.32 and $\Lambda_{HA\text{-}i\text{-}PEA}$=1.20; this means volume swelling ratios of Λ^3_{PEA}=1.00, Λ^3_{HA}=2.29 and $\Lambda^3_{HA\text{-}i\text{-}PEA}$=1.73. Besides, the use of FBS in the culture media, which was also used in the conditioning of samples prior to cell seeding, improves cell adhesion on HA due to the presence of soluble fibronectin[40-42] which might be attached to the surface and act as an adhesive molecule for cells. This effect could be enhanced in HA scaffolds, as these two molecules have shown good results when combined as a substrate for fibroblast growth.[10, 42-43] Finally, the creation of micro-textures on the surfaces of HA during lyophilization could have a positive influence on cell adhesion, according to the literature.[20, 35-37] IPN samples seem to achieve slightly higher cell proliferation values than the single network scaffolds at day 5 and day 10.

SEM images from these cultures at day 10 (Figure 7) reveal that cells grow attached to the inner surface of the scaffold pores in all materials, while forming a tight continuous layer. Cells show a packed, spherical morphology on all the scaffolds, without remarkable differences between HA, PEA and IPN ones. Immunofluorescent imaging of actin cytoskeletons (Figure 8) reveals differences between all three materials at day 10. In PEA scaffolds, cells are well-spread and show a clearly defined actin cytoskeleton with multiple stress fibers (Figure 8A and 8A'). In HA scaffolds, cells are spindle-shaped, tightly packed

and aligned; with lined up stress fibers, albeit poorly defined, and multiple actin patches (Figure 8B and 8B'). In IPN (HA-i-PEA) scaffolds, cells are also aligned and packed, but actin distribution is less patched, with more stress fibers than those seen in HA scaffold cultures (Figure 8C and 8C'). These differences allow distinguishing the effects of each material on cell growth and attachment, as both cell adhesion and cell motility depend on the polymerization and distribution of actin throughout the cells. The highly hydrophobic surface of PEA scaffolds seems to promote an extended morphology of fibroblast cells, which develop an intense cytoskeleton of long polymeric actin fibers, typical of stiff substrates;[44-45] this kind of morphology may limit further cell proliferation on the available surface due to cell-cell contact inhibition, as seen in the MTS assay. In HA scaffolds, actin patches throughout cytoplasmatic areas reveal a dynamic state of cell cytoskeleton, which is compatible with this kind of substrate as it promotes cell motility; or at least focal adhesion turnover through RHAMM receptors.[13, 45] The observed actin patches usually form in earlier stages of formation of the actin cytoskeleton, during actin polymerization near the cytoplasmatic side of substrate-adherent integrins, in processes of cell adhesion and migration via lamellipodia.[46] Usually, these patches disappear rapidly after they form, as actin clusters merge and travel in waves until they reach the cell borders, expanding the substrate-attached cell surface from there and allowing for cell spreading.[47] However, actin patches in HA samples are seen simultaneously with stress fibers. This can be explained by the fact that the creation of focal adhesions is compatible with fibroblasts growing in such substrate after reaching confluence, when cells are allowed to adhere to each other, thus overcoming many adverse effects derived from the substrate's low stiffness and high water content.[45, 48]

According to this, these cells may show both stress fibers derived from cell-cell adhesion, and an arrested (or even active) process of adhesion (or migration) derived from cell-substrate interactions. In HA-i-PEA scaffolds, fibroblast cells do not show these actin patches as profusely as in HA and, by contrast, they show more oriented long actin filaments, or stress

fibers, as was the case in PEA. The presence of both HA and PEA as substrates for cell adhesion would lead to *durotaxis*, the migration of cells towards a stiffer surface (PEA), but again this may be overcome after cell confluence is achieved, as in HA. However, unlike in HA scaffolds, some parts of the cell monolayer do have a stiff and adherent substrate where they can be firmly attached, and then transmit tensile stress to the rest of cells via the extracellular matrix.[49] Thus, IPN scaffolds yield cell cultures which combine the high colonization density of HA scaffolds with a high proportion of cells having a mature actin cytoskeleton akin to PEA scaffolds.

4. Conclusions

The combination of two very different polymers such as hyaluronic acid and poly(ethyl acrylate) in the form of interpenetrating networks led to biphasic materials retaining the physicochemical properties of both components. A procedure involving the template-leaching technique was developed in order to fabricate porous scaffolds from these IPN. Highly porous scaffolds with a regularly interconnected porous structure were obtained. Absence of cytotoxicity of the new materials was assessed by direct and indirect tests with fibroblast cultures. Cell invasion and colonization of the scaffolds was similar in the case of the three types of scaffolds, with some differences attributable to the available space for cells in each scaffold type. Differences were more significant regarding the way cells attached to the scaffolds. Within PEA scaffolds, cells were attached on the surface with a spread out morphology and a strong and well defined actin cytoskeleton. Actin cytoskeleton was less defined in the case of cells cultured on HA scaffolds, which relates to a weaker cell-material interaction. On HA-i-PEA scaffolds, cells display a well defined actin cytoskeleton, nearly as defined as cells on PEA. This excellent biological performance combining features of both PEA and HA is accompanied by tunable mechanical properties, degradability and

swellability, achieved by changing the parameters of HA crosslinking and lyophilization, in order to create a sufficiently interconnected porous network before PEA polymerization, and EA monomer concentration. The authors think that these novel materials could facilitate very promising cell culture systems for tissue engineering applications.

Appendix/Nomenclature/Abbreviations

DVS : divinyl sulfone

EA : ethyl acrylate

EGDMA : ethylene glycol dimethacrylate

HA : hyaluronic acid (sodium salt)

HA-i-PEA : hyaluronic acid and poly(ethyl acrylate) interpenetrating polymer networks

IPN : interpenetrating polymer networks

PEA : poly(ethyl acrylate)

PEMA : poly(ethyl methacrylate)

PMMA : poly(methyl methacrylate)

WC / EWC : water content / equilibrium water content

Acknowledgements: Support of this work through projects PRI-PIMNEU-2011-1372 (ERANET-Neuron) and CICyT MAT2011-28791-C03-02 is gratefully acknowledged. The authors would like to thank PhD. Carmen Antolinos and PhD. Keila Alvarado for their assistance in the TMA assay. Assistance and advice received from the Electron Microscopy Service at the Universitat Politècnica de València is also acknowledged.

Received: Month XX, XXXX; Revised: Month XX, XXXX; Published online:

((For PPP, use "Accepted: Month XX, XXXX" instead of "Published online")); DOI: 10.1002/marc.((insert number)) ((or ppap., mabi., macp., mame., mren., mats.))

Keywords: biomaterials; hyaluronic acid; interpenetrating networks (IPN); poly(ethyl acrylate); scaffolds

[1] Y. Ikada, *J R Soc Interface* **2006,** *3*, 589.

[2] H. Shin; S. Jo; A. G. Mikos, *Biomaterials* **2003,** *24*, 4353.

[3] P. L. Bollyky; J. D. Lord; S. A. Masewicz; S. P. Evanko; J. H. Buckner; T. N. Wight; G. T. Nepom, *J. Immunol.* **2007,** *179*, 744.

[4] P. H. Weigel; S. J. Frost; C. T. McGary; R. D. LeBoeuf, *Int. J. Tissue React.* **1988,** *10*, 355.

[5] P. H. Weigel; G. M. Fuller; R. D. LeBoeuf, *J. Theor. Biol.* **1986,** *119*, 219.

[6] M. J. Kujawa; D. G. Pechak; M. Y. Fiszman; A. I. Caplan, *Dev. Biol.* **1986,** *113*, 10.

[7] C. K. Perng; Y. J. Wang; C. H. Tsi; H. Ma, *J. Surg. Res.* **2011,** *168*, 9.

[8] P. W. Noble, *Matrix Biol.* **2002,** *21*, 25.

[9] G. Abatangelo; M. Martelli; P. Vecchia, *J. Surg. Res.* **1983,** *35*, 410.

[10] E. Zimmerman; B. Geiger; L. Addadi, *Biophys. J.* **2002,** *82*, 1848.

[11] E. A. Turley; P. W. Noble; L. Y. Bourguignon, *J. Biol. Chem.* **2002,** *277*, 4589.

[12] M. Morra, *Biomacromolecules* **2005,** *6*, 1205.

[13] C. L. Hall; C. Wang; L. A. Lange; E. A. Turley, *J. Cell Biol.* **1994,** *126*, 575.

[14] T. Fujii; Y. L. Sun; K. N. An; Z. P. Luo, *J. Biomech.* **2002,** *35*, 527.

[15] O. Jeon; S. J. Song; K.-J. Lee; M. H. Park; S.-H. Lee; S. K. Hahn; S. Kim; B.-S. Kim, *Carbohydrate Polymers* **2007,** *70*, 251.

[16] F. Z. Cui; W. M. Tian; S. P. Hou; Q. Y. Xu; I. S. Lee, *Journal of materials science. Materials in medicine* **2006,** *17*, 1393.

[17] S. Hou; Q. Xu; W. Tian; F. Cui; Q. Cai; J. Ma; I. S. Lee, *J. Neurosci. Methods* **2005,** *148*, 60.

[18] S. K. Seidlits; Z. Z. Khaing; R. R. Petersen; J. D. Nickels; J. E. Vanscoy; J. B. Shear; C. E. Schmidt, *Biomaterials* **2010,** *31*, 3930.

[19] D. Eng; M. Caplan; M. Preul; A. Panitch, *Acta Biomaterialia* **2010,** *6*, 2407.

[20] S. Ibrahim; Q. K. Kang; A. Ramamurthi, *J Biomed Mater Res A* **2010,** *94*, 355.

[21] M. Mensitieri; L. Ambrosio; L. Nicolais; D. Bellini; M. O'Regan, *J Mater Sci: Mater Med* **1996,** *7*, 695.

[22] Y. D. Sanzgiri; E. M. Topp; L. Benedetti; V. J. Stella, *Int. J. Pharm.* **1994,** *107*, 91.

[23] S. A. Bencherif; A. Srinivasan; F. Horkay; J. O. Hollinger; K. Matyjaszewski; N. R. Washburn, *Biomaterials* **2008,** *29*, 1739.

[24] L. Cen; K. G. Neoh; Li; E. T. Kang, *Biomacromolecules* **2004,** *5*, 2238.

[25] J. J. Campbell; N. Davidenko; M. M. Caffarel; R. E. Cameron; C. J. Watson, *PLoS One* **2011,** *6*, e25661.

[26] H. L. Frisch, *British Polymer Journal* **1985,** *17*, 149.

[27] J. M. Soria; C. Martinez Ramos; O. Bahamonde; D. M. Garcia Cruz; M. Salmeron Sanchez; M. A. Garcia Esparza; C. Casas; M. Guzman; X. Navarro; J. L. Gomez Ribelles; J. M. Garcia Verdugo; M. Monleon Pradas; J. A. Barcia, *J Biomed Mater Res A* **2007,** *83*, 463.

[28] M. Perez Olmedilla; N. Garcia-Giralt; M. M. Pradas; P. B. Ruiz; J. L. Gomez Ribelles; E. C. Palou; J. C. Garcia, *Biomaterials* **2006,** *27*, 1003.

[29] C. Martínez-Ramos; S. Lainez; F. Sancho; M. A. García Esparza; R. Planells-Cases; J. M. García Verdugo; J. L. Gómez Ribelles; M. Salmerón Sánchez; M. Monleón Pradas; J. A. Barcia; J. M. Soria, *Tissue Engineering Part A* **2008,** *14*, 1365.

[30] C. Martinez-Ramos; A. Valles-Lluch; J. M. Verdugo; J. L. Ribelles; J. A. Barcia Albacar; A. B. Orts; J. M. Soria Lopez; M. M. Pradas, *J Biomed Mater Res A* **2012,** *100*, 3276.

[31] J. L. Alio del Barrio; M. Chiesa; G. Gallego Ferrer; N. Garagorri; N. Briz; J. Fernandez-Delgado; M. Sancho-Tello Valls; C. C. Botella; I. Garcia-Tunon; L. Bataille; A. Rodriguez; F. Arnalich-Montiel; J. L. Gomez Ribelles; C. M. Antolinos-Turpin; J. A. Gomez-Tejedor; J. L. Alio; M. P. De Miguel, *J Biomed Mater Res A* **2015,** *103*, 1106.

[32] J. Schindelin; I. Arganda-Carreras; E. Frise; V. Kaynig; M. Longair; T. Pietzsch; S. Preibisch; C. Rueden; S. Saalfeld; B. Schmid; J. Y. Tinevez; D. J. White; V. Hartenstein; K. Eliceiri; P. Tomancak; A. Cardona, *Nature methods* **2012,** *9*, 676.

[33] A. Ramamurthi; I. Vesely, *J Biomed Mater Res A* **2003,** *66*, 317.

[34] M. M. Doherty; P. J. Hughes; S. R. Kim; D. E. Mainwaring; W. N. Charman, *Int. J. Pharm.* **1994,** *111*, 205.

[35] D. Wedlock; G. Phillips; A. Davies; J. Gormally; E. Wyn-Jones, *Int. J. Biol. Macromol.* **1983,** *5*, 186.

[36] Y. Tokita; K. Ohshima; A. Okamoto, *Polymer Degradation and Stability* **1997,** *55*, 159.

[37] V. R. Patel; M. M. Amiji, *Pharm. Res.* **1996,** *13*, 588.

[38] L. H. Sperling, *Interpenetrating polymer networks and related materials*. Springer Science & Business Media: 2012.

[39] E. A. Turley, *Cancer Metastasis Rev.* **1984,** *3*, 325.

[40] M. S. Lord; D. Pasqui; R. Barbucci; B. K. Milthorpe, *J Biomed Mater Res A* **2009,** *91*, 635.

[41] A. Ramamurthi; I. Vesely, *J. Biomed. Mater. Res.* **2002,** *60*, 195.

[42] F. Grinnell; M. K. Feld, *J. Biol. Chem.* **1982,** *257*, 4888.

[43] K. Ghosh; X.-D. Ren; X. Z. Shu; G. D. Prestwich; R. A. Clark, *Tissue Eng.* **2006,** *12*, 601.

[44] J. Solon; I. Levental; K. Sengupta; P. C. Georges; P. A. Janmey, *Biophys. J.* **2007,** *93*, 4453.

[45] T. Yeung; P. C. Georges; L. A. Flanagan; B. Marg; M. Ortiz; M. Funaki; N. Zahir; W. Ming; V. Weaver; P. A. Janmey, *Cell Motil. Cytoskeleton* **2005,** *60*, 24.

[46] G. Gerisch; T. Bretschneider; A. Müller-Taubenberger; E. Simmeth; M. Ecke; S. Diez; K. Anderson, *Biophys. J.* **2004,** *87*, 3493.

[47] O. Collin; P. Tracqui; A. Stephanou; Y. Usson; J. Clément-Lacroix; E. Planus, *J. Cell Sci.* **2006,** *119*, 1914.

[48] C.-M. Lo; H.-B. Wang; M. Dembo; Y.-l. Wang, *Biophys. J.* **2000,** *79*, 144.

[49] N. Wang; J. D. Tytell; D. E. Ingber, *Nature reviews Molecular cell biology* **2009,** *10*, 75.

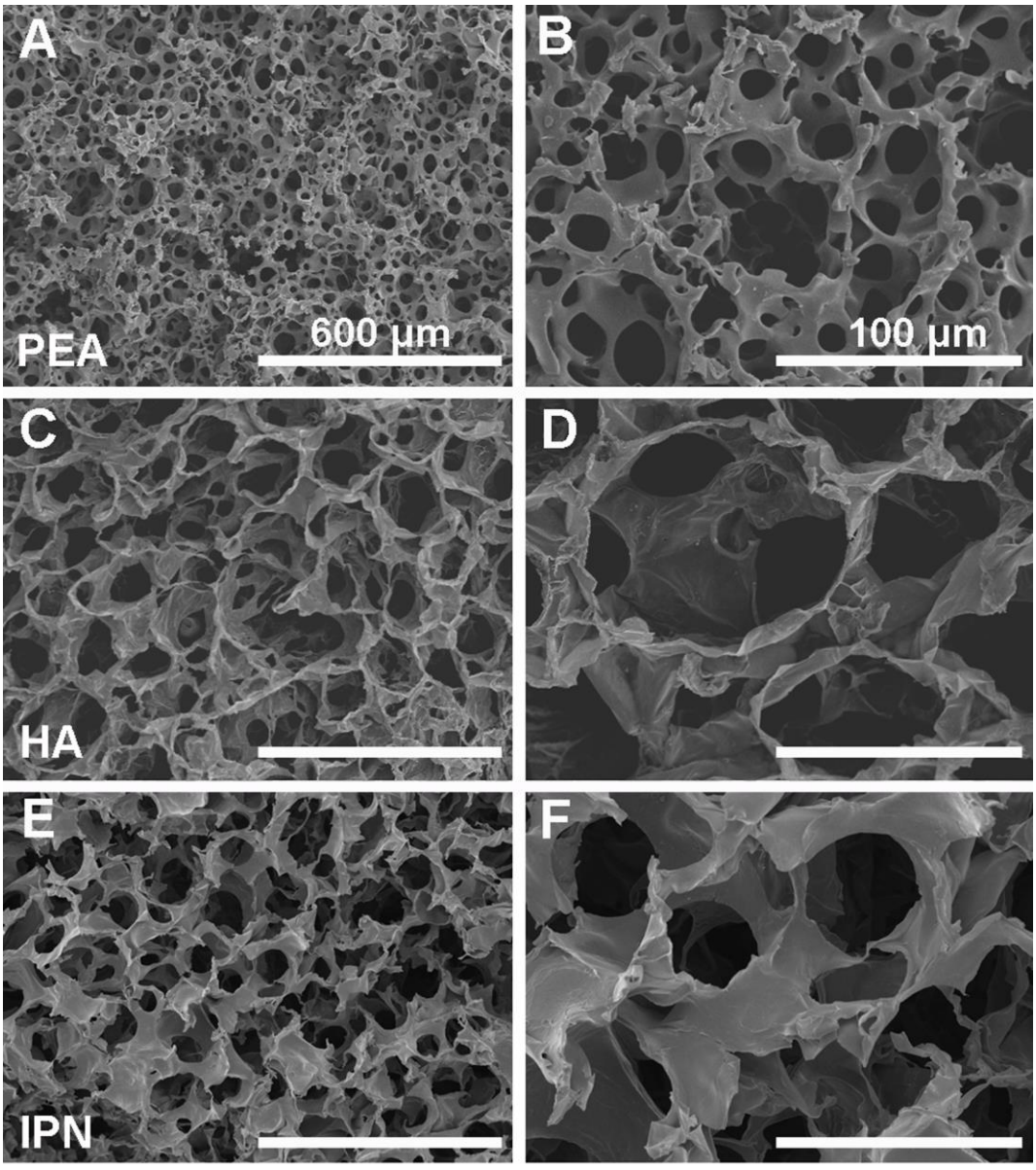

Figure 1. Scanning electron micrographs obtained from PEA (A and B), HA (C and D) and the HA-i-PEA (IPN) (E and F) scaffolds.

Table 1. Properties of PEA, HA and HA-i-PEA (IPNs) scaffolds.

	HA	**PEA**	**HA-i-PEA**
Pore diameter (μm)	174±32	104±18	182±20
Thickness (dry) (mm)	2.07±0.05	1.26±0.11	1.89±0.10
Thickness (swollen) (mm)	2.73±0.22	1.26±0.11	2.27±0.07
Density (ρ) (g/cm^3)	0.94±0.12	1.13±0.01	1.00±0.16
Porosity (Ø) (%)	95.85±0.32	61.79±6.62	96.87±2.16
E.W.C. (scaff.) $(m_{eq}-m_0)/m_0$	78.06±9.31	2.53±0.80	66.39±5.58
Tensile Young Modulus (MPa)	0.05±0.02	0.83±0.09	0.28±0.04
PEA mass fraction from TGA (%)	-	-	23.4±4.4
PEA mass fraction from EDS (%)	-	-	23.2±0.4

Table 2. EDS analysis showing quantitative values for N and Na atoms (%) obtained from PEA, IPN and HA scaffolds.

	N atom (%)	**Na atom (%)**
HA	4.4±1.2	5.6±0.1
PEA	0.1±0.1	0
HA-i-PEA	3.4±0.7	4.2±0.2

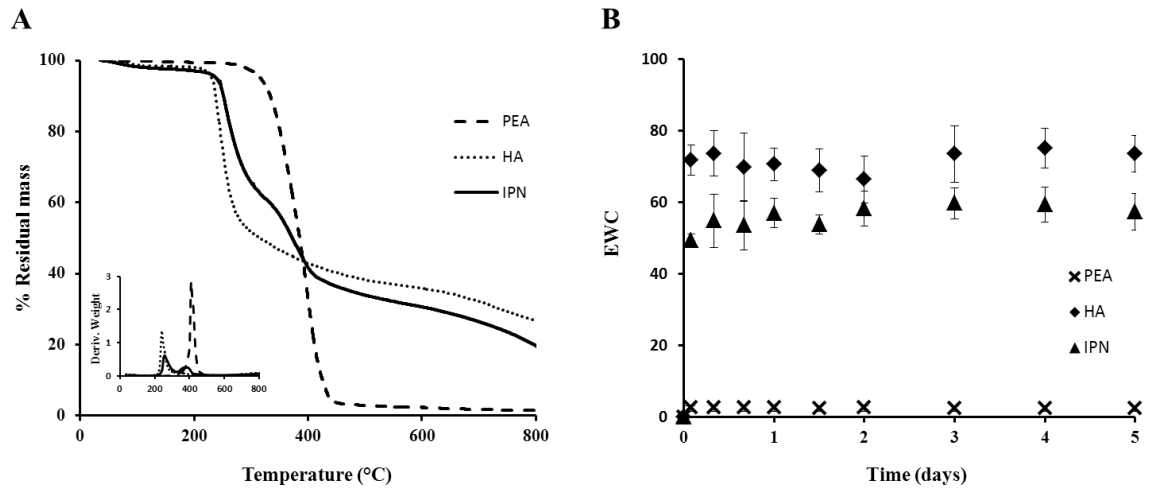

Figure 2. Thermogravimetry (A) and dynamic swelling (B) of PEA, HA and IPN materials. A: Residual weight versus temperature expressed as percentage of the initial mass, and the temperature rate of the weight loss (insert). B: Swelling ratio as a function of time in immersion experiments.

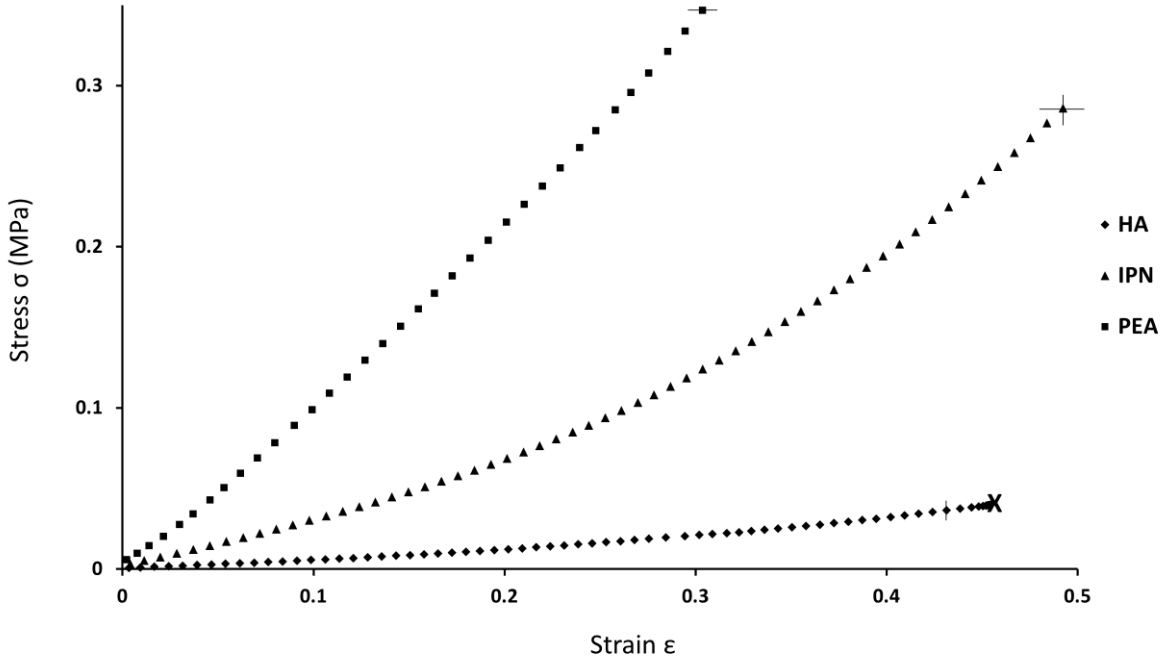

Figure 3. Tensile stress response of PEA, HA and IPN under constant stretching rate of 5 $mm \cdot min^{-1}$. The "X" symbol next to HA series indicates that samples broke near that point.

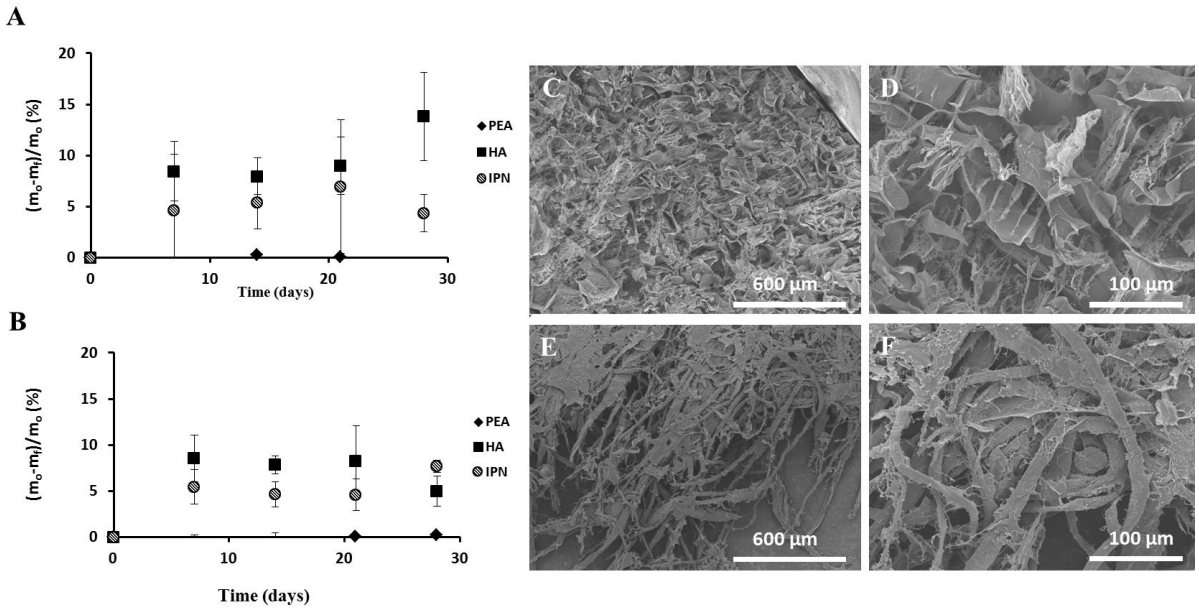

Figure 4. Degradation of PEA, HA and IPN materials. Percentage of weight lost against time of immersion in HAse medium (A) and in PBS (B). CryoSEM images of swollen HA-i-PEA (IPN) scaffolds (C, D), and of the same materials after a fast degradation in an extremely low pH medium (E, F).

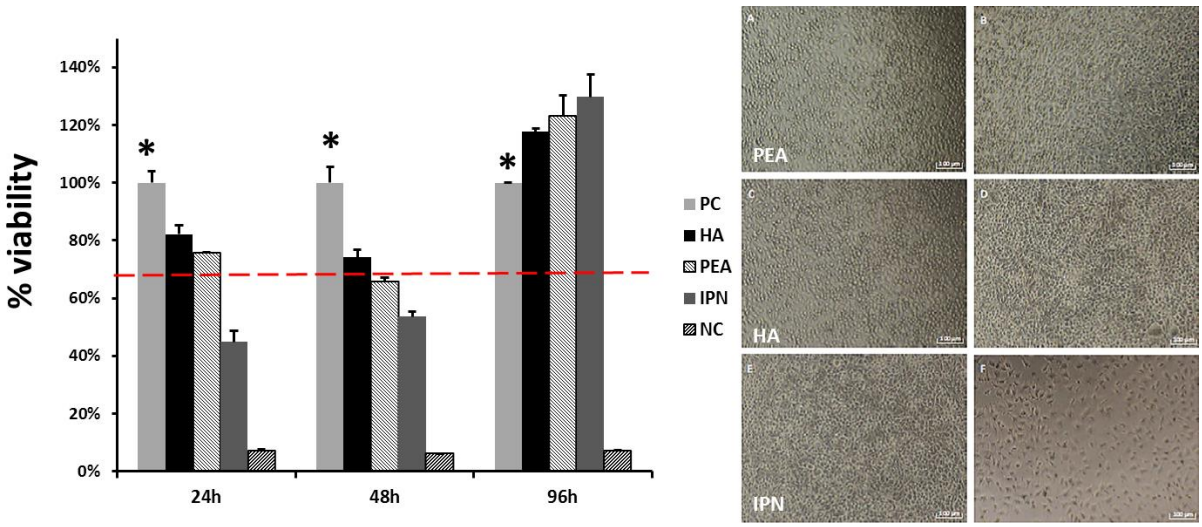

Figure 5. Cell viability on PEA, HA and IPN materials. Plot: absorbance in MTT tests of cell cultures of L929 fibroblasts with extracts from the materials, referred to the positive control (PC, see text) after 24, 48, and 72 h of culture. Images obtained in a light microscope corresponding to the same cultures at 72h, including the blank (A), PC (B), PEA extracts (C),

HA extracts (D), IPN extracts (E), and the negative control NC (F). * P < 0.05 when compared to others groups.

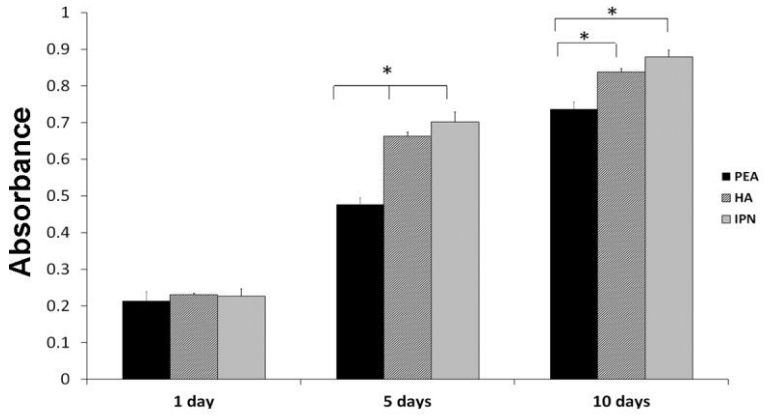

Figure 6. Proliferation and adhesion of cells in PEA, HA and IPN scaffolds. Plot: MTS absorbance test for cultures of L929 fibroblasts after 1, 5 and 10 days. * P < 0.05.

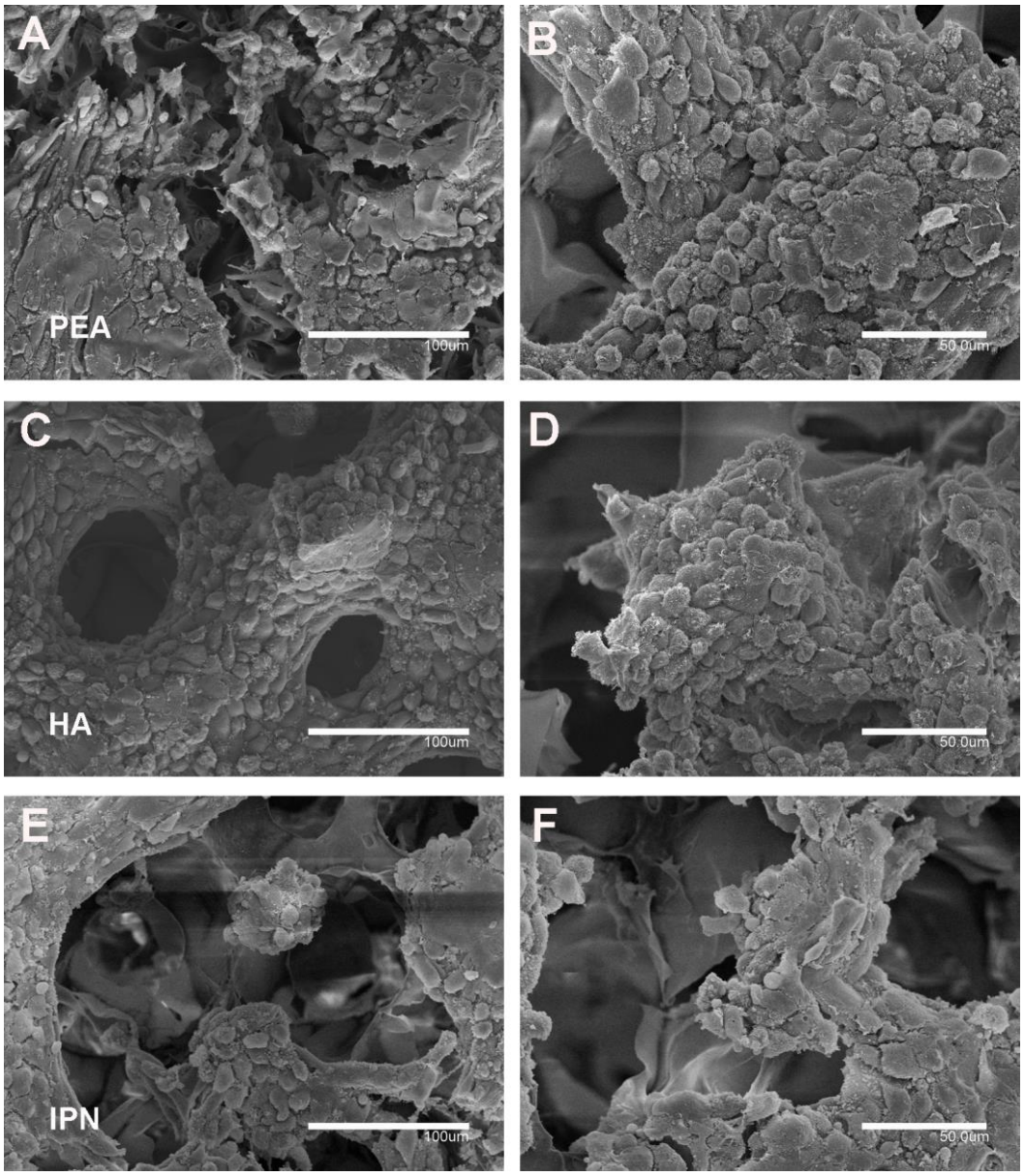

Figure 7. SEM images of L929 cultures on the 10th day in PEA (A, B), HA (C, D) and IPN scaffolds (E, F). Scale bars: 100 µm (A, C, E) and 50 µm (B, D, F).

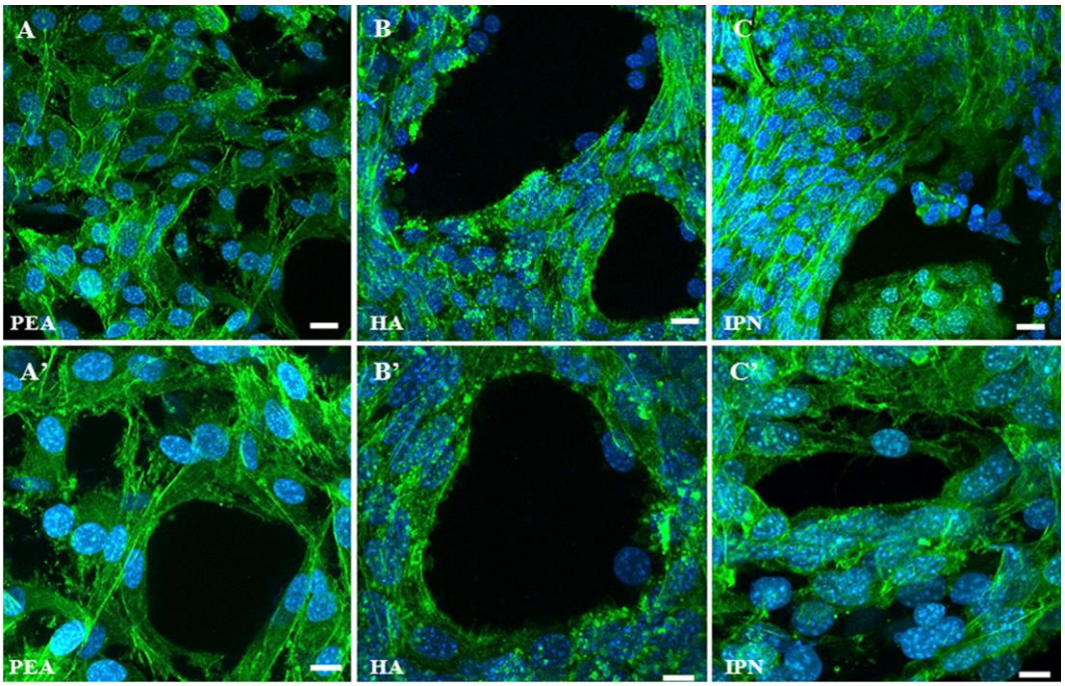

Figure 8. CSLM images of L929 cultures on the 10th day immunostained with phallacidin in PEA (A, A'), HA (B, B') and IPN scaffolds (C, C'). Actin fibers show different states of cell activity (adhesion, cell migration and proliferation) by changing the shape of the fibers: more extended on PEA scaffold and more stress fibers on HA.

Interpenetrating networks of hyaluronic acid (HA) and poly(ethyl acrylate) (PEA) are prepared in the shape of porous scaffolds through a template-leaching technique; combining properties of these two materials. Both physicochemical and biological responses of these IPN scaffolds are studied, including their cytotoxicity and their effects in cell proliferation and attachment; comparing them to those of HA and PEA porous single-network scaffolds.

E. Rodríguez-Pérez, A. Lloret Compañ, M. Monleón Pradas*, C. Martínez-Ramos.

Scaffolds of hyaluronic acid-poly(ethyl acrylate) interpenetrating networks: characterization and in vitro studies

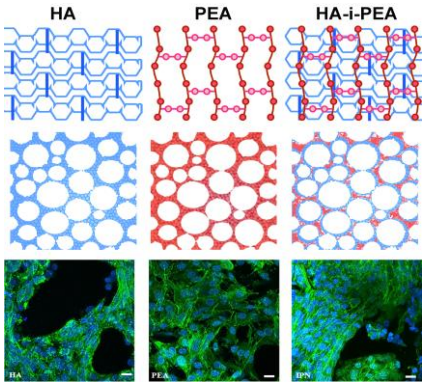

Supporting Information

for *Macromol. Biosci.*, DOI: 10.1002/mabi.2013#####

Scaffolds of hyaluronic acid-poly(ethyl acrylate) interpenetrating networks: characterization and in vitro studies

E. Rodríguez-Pérez, A. Lloret Compañ, M. Monleón Pradas*, C. Martínez-Ramos.